Mohsen Akbari[1]
Ph.D. Candidate
Mechatronic System Engineering,
School of Engineering Science,
Simon Fraser University,
Surrey, BC, V3T 0A3, Canada
e-mail: maa59@sfu.ca

David Sinton
Associate Professor
Department of Mechanical Engineering,
University of Victoria,
Victoria, BC, V8W 2Y2, Canada

Majid Bahrami
Assistant Professor
Mem. ASME
Mechatronic System Engineering,
School of Engineering Science,
Simon Fraser University,
Surrey, BC, V3T 0A3, Canada

Pressure Drop in Rectangular Microchannels as Compared With Theory Based on Arbitrary Cross Section

Pressure driven liquid flow through rectangular cross-section microchannels is investigated experimentally. Polydimethylsiloxane microchannels are fabricated using soft lithography. Pressure drop data are used to characterize the friction factor over a range of aspect ratios from 0.13 to 0.76 and Reynolds number from 1 to 35 with distilled water as working fluid. Results are compared with the general model developed to predict the fully developed pressure drop in arbitrary cross-section microchannels. Using available theories, effects of different losses, such as developing region, minor flow contraction and expansion, and streaming potential on the measured pressure drop, are investigated. Experimental results compare well with the theory based on the presure drop in channels of arbitrary cross section. [DOI: 10.1115/1.3077143]

1 Introduction

Advances in microfabrication make it possible to build microchannels with micrometer dimensions. Micro- and minichannels show potential and have been incorporated in a wide variety of unique, compact, and efficient cooling applications in microelectronic devices [1]. These microheat exchangers or heat sinks feature extremely high heat transfer surface area per unit volume ratios, high heat transfer coefficients, and low thermal resistances. In biological and life sciences, microchannels are used widely for analyzing biological materials such as proteins, DNA, cells, embryos, and chemical reagents [2]. Various microsystems, such as microheat sinks, microbiochips, microreactors, and micronozzles have been developed in recent years [3–6]. Since microchannels are usually integrated into these microsystems, it is important to determine the characteristics of the fluid flow in microchannels for better design of various microflow devices.

In parallel to the recent advances in microfluidic devices, microfabrication techniques have evolved. Some of the important fabrication techniques include lithography (soft and photolithography), lamination, injection molding, hot embossing, laser micromachining, and electrochemical or ultrasonic technologies [2,7–10]. Together with new methods of fabrication, it is possible to exploit certain fundamental differences between the physical properties of fluids moving in large channels and those traveling through micrometer-scale channels [2]. In recent years, a large number of papers have reported pressure drop data for laminar fully developed flow of liquids in microchannels with various cross sections [11–32]. Rectangular cross sections have been extensively studied as they are employed in many applications [11–16]. However, published results are often inconsistent. Some authors reported a huge deviation from the conventional theories and attributed it to an early onset of laminar to turbulent flow transition or surface phenomena such as surface roughness, electrokinetic forces, viscous heating effects, and microcirculation near the wall [12–26].

Jiang et al. [28] conducted an experimental investigation of water flow through different microchannel cross sections including circular, rectangular, trapezoidal, and triangular. The hydraulic diameter of microchannels varied from 8 μm to 42 μm. They collected experimental data with the Reynolds number ranging from 0.1 to 2, and concluded that there was less influence of the cross-sectional shape on the microflow in the microchannel and that the experimental data agreed well with the prediction of the conventional theory. Baviere et al. [29] performed an experimental study on the water flow through smooth rectangular microchannels. Their channels were made of a silicon engraved substrate anodically bonded to a Pyrex cover. Their results showed that in smooth microchannels, the friction law is correctly predicted by conventional theories. Judy et al. [15] and Bucci et al. [30] showed that their experimental results were in good agreement with conventional theories in the laminar regime. Also Wu and Cheng [31], Liu and Garimella [32], and Gao et al. [33] reported good agreement between experimental data with conventional theories.

Low Reynolds numbers characterize many microscale liquid flows [34]. Hence, nonlinear terms in the Navier–Stokes equation disappear for fully developed flow, resulting in Poisson's equation

$$\nabla^2 u = \frac{1}{\mu}\frac{dp}{dz}, \quad u = 0 \text{ on } \Gamma \tag{1}$$

where u is the fluid velocity, z is the flow direction, and Γ is the perimeter of the channel. Exact solution for Eq. (1) in rectangular cross-section channels can be found in fluid mechanics textbooks such as Ref. [35]. The original analytical solution for the mean velocity in rectangular channels is in the form of a series, but it has been shown that using the first term of the series results in errors less than 0.7%.

Recently, Bahrami et al. [1,36] developed a general model for prediction of pressure drop in microchannels of arbitrary cross section. Using the analytical solution of elliptical duct and the concept of Saint-Venant principal in torsion [37], they showed that the Poiseuille number, $f\ \mathrm{Re}_{\sqrt{A}}$, is a function of the polar moment of inertia, I_P, area, A, and perimeter of the cross section of the channel, Γ. Their model showed good agreement with experimental and numerical data for a wide variety of channel cross sections such as rectangular, trapezoidal, triangular, circular, and moon shaped.

[1]Corresponding author.

Contributed by the Fluids Engineering Division of ASME for publication in the JOURNAL OF FLUIDS ENGINEERING. Manuscript received June 11, 2008; final manuscript received December 5, 2008; published online March 6, 2009. Assoc. Editor: James A. Liburdy. Paper presented at the ECI International Conference on Heat Transfer and Fluid Flow in Microscale III, Whistler, BC, Canada, September 21–26, 2008.

However, they [1,36] did not perform any experiment to verify this model, thus they could not investigate all issues and effects of different parameters. As a result the goal of the present work is to independently validate the general model of Bahrami et al. [1,36]. Moreover, effects of different parameters, including microchannel dimensions, minor and developing region losses, viscous heating, electroviscous phenomena, and channel deformation on the measured pressure drop, have been discussed. By successfully validating the model, it will be used in more complicated channel geometries such as variable cross-section microchannels.

2 Theory

Selection of the characteristic length is an arbitrary choice and will not affect the final solution. However, an appropriate length scale leads to more consistent results, especially when a general cross section is considered. A circular duct is fully described with its diameter, thus the obvious length scale is the diameter (or radius). For noncircular cross sections, the selection is not as clear; many textbooks and researchers have conventionally chosen the hydraulic diameter as the characteristic length. Yovanovich [38] introduced the square root of area as a characteristic length scale for heat conduction and convection problems. Later, Muzychka and Yovanovich [39] proposed the use of $\sqrt{A}$ for the fully developed flow in noncircular ducts. Bahrami et al. [1,37] showed that the square root of area appears in the solution of fully developed flow in noncircular ducts. They also compared both D_h and $\sqrt{A}$ and observed that using $\sqrt{A}$ as the characteristic length scale results in similar trends in Poiseuille number for microchannels with a wide variety of cross sections. Therefore, in this study, $\sqrt{A}$ is selected consistently as the length scale throughout the analysis.

According to the model of Bahrami et al. [1], pressure drop of laminar fully developed flow in arbitrary cross-section microchannels can be obtained from

$$\Delta P = 16\pi^2 \mu Q I_p^* \frac{L}{A^2} \tag{2}$$

where $I_p^* = I_p/A$ is the specific polar momentum of inertia of the microchannel cross section, $\Gamma = 4(W+H)$ is the microchannel cross-section perimeter, L is the fully developed length, and Q is the the volumetric flow rate. Substituting for the geometrical parameters in Eq. (2) for microchannels of rectangular cross section and the definition of the Poiseuille number yields [1]

$$f\ \mathrm{Re}_{\sqrt{A}} = \frac{4\pi^2(1+\varepsilon^2)}{3\sqrt{\varepsilon}(1+\varepsilon)} \tag{3}$$

As can be seen the only parameter effects the Poiseuille number in rectangular channels is the cross-section aspect ratio, consistent with previous works [35,40]. For rectangular microchannels, two asymptotes can be recognized, i.e., very narrow rectangular and square channels

$$f\ \mathrm{Re}_{\sqrt{A}} = \frac{4\pi^2}{3\sqrt{\varepsilon}}; \quad \varepsilon \to 0$$

$$f\ \mathrm{Re}_{\sqrt{A}} = 13.16; \quad \varepsilon = 1 \tag{4}$$

3 Experimental Setup

3.1 Chemicals and Materials. De-ionized water was used as the testing liquid. SU-8 photoresist (Microchem, Newton, MA) and diacetone-alcohol developer solution (Sigma-Aldrich, St. Louis, MO) were used in the making of the positive relief masters by the procedure outlined below. Polydimethylsiloxane (PDMS) casts were prepared by thoroughly mixing the base and curing agent at a 10:1 ratio as per the manufacturer's instructions for the Sylgard 184 silicon elastomer kit (Dow Corning, Midland, MI). Caution was used to avoid contact between the liquid PDMS and latex rubber (gloves), as this was found to inhibit curing [41].

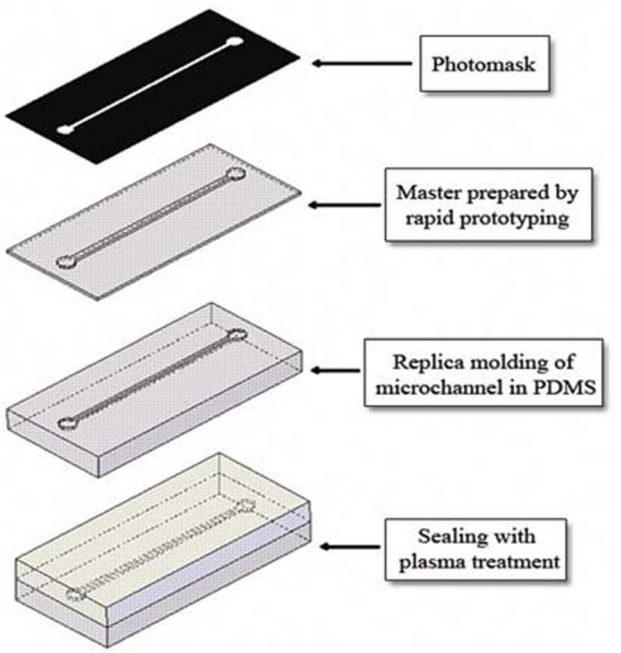

Fig. 1 Schematic of the soft lithography technique

3.2 Microfabrication. The PDMS/PDMS microchannels used in this study have been manufactured using the soft lithography technique [42] described by Erickson et al. [41]. A schematic of the process is provided in Fig. 1. Photomasks were designed by AUTOCAD software[2] and printed with a 3500DPI printer (Island Graphics Ltd., Victoria, BC, Canada). Masters containing the desired microchannel pattern have been made by spin coating of SU-8 negative photoresist on a glass slide to the desired thickness. The photoresist film was then hardened through a two-stage direct contact pre-exposure bake procedure (65 °C for 5 min and 95 °C for 30 min) and exposed to UV light for 100 s through the mask containing the channel pattern. A two-stage postexposure bake procedure (65 °C for 5 min and 95 °C for 30 min) was then used to enhance cross linking in the exposed portion of the film. The slide was then placed in quiescent developer solution for 10 min to dissolve the unexposed photoresist, leaving a positive relief containing the microchannel pattern.

Liquid PDMS was then poured over the master and exposed to vacuum condition (1 h) to extract all the bubbles in it and cured at 85 °C for 15–20 min yielding a negative cast of the microchannel pattern. An enclosed microchannel was then formed by bonding the PDMS cast with another piece of PDMS via plasma treatment.

Five microchannels were made with a range of aspect ratios, $0.13 < \varepsilon < 0.76$, and tested in this study. Dimensions of the microchannels are shown in Table 1. The channels' names in the table indicate the channel material, cross-sectional shape, and the aspect ratio (i.e., PPR-0.13 corresponds to the PDMS/PDMS chip with rectangular cross section and the aspect ratio of 0.13). As can be seen, channels were designed long enough so that fully developed flow is dominant. Since the microchannel dimensions have a major effect on the friction factor calculation [13,15,33], a destructive careful measurement was performed after the experiments. Channels were cut carefully at three random cross sections. The cutting lines were perpendicular to the channel to ensure a 90 deg viewing angle. Dimensions of the channel were measured by an image processing method. To do so, a Leica DMI 6000B (Leica Microsystems, Richmond Hill, ON, Canada) microscope with a 10×, 0.4 N.A. objective was used. Images of the channel cross

[2] www.usa.autodesk.com.

Table 1 Dimensions of the fabricated microchannels

Channel	Width, $2W$ (μm)	Depth, $2H$ (μm)	Length, L (mm)	$\varepsilon = H/W$	$L_{D,\max}/L$ (%)
PPR-0.13	780	110	50	0.13	3.47
PPR-0.17	581	101	50	0.17	4.03
PPR-0.4	480	192	58.8	0.4	5.55
PPR-0.6	189	113	55.5	0.6	6.75
PPR-0.76	134	103	50	0.76	7.86

section were captured by a high resolution high sensitivity CCD camera (Hamamatsu Orca AG, NJ) and imported into a photo editing software, ADOBE PHOTOSHOP 8.0. Dimensions of the channel were then measured by pixel counting. Size of each pixel was calibrated using a known dimension provided by the microscope image acquisition software. Accuracy of this method was found to be ± 3.6 μm. Due to the microfabrication process, the microchannel cross section has some deviations from the rectangular shape. Height and width measurements were conducted at different random positions for each cross section and the average value was determined. This measurement was also performed at several cross sections. Mean values are reported in Table 1. It was observed that both microchannel depth and width were different from the expected values in the fabrication process. From our measurements, channel height, and width deviated less than 4% and 3% from the designed sizes, respectively. Since smooth surfaces were observed by the image processing technique described above, the roughness of the channels was estimated to be less than the accuracy of the image processing method. Hence, the relative channel roughness (channel roughness/channel length scale) was found to be less than 3%. As a result the effect of roughness on the pressure drop of the fully developed flow can be neglected [27].

3.3 Experimental Procedure. An open loop syringe pump system, as illustrated in Fig. 2, was designed for this work. A syringe pump (Harvard Apparatus, QC, Canada) provided constant flow rate with $\pm 0.5\%$ accuracy. A range of Reynolds numbers was covered by changing the volumetric flow rate from 40 μl/min to 240 μl/min. Water was forced to flow through a submicron filter (Aktreingeselchaf Co., Germany) before entering the channel. To measure the pressure drop, a gauge pressure transducer (Omega Inc., Laval, QC, Canada) was fixed at the channel inlet while the channel outlet was opened to the atmosphere. Teflon tubing (Scientific Products And Equipment, North York, ON, Canada) was employed to connect the pressure transducer to the syringe pump and the microchannel. Measured pressure was then monitored and recorded with a computerized data acquisition system (LABVIEW 8.5, National Instruments, USA[3]). The flow was considered to have reached a steady state condition when the readings of the pressure drop did not change with time. For a given channel, the measurement of pressure drop was repeated three times for each flow rate. An arithmetic averaging method [43] was performed to determine the final results.

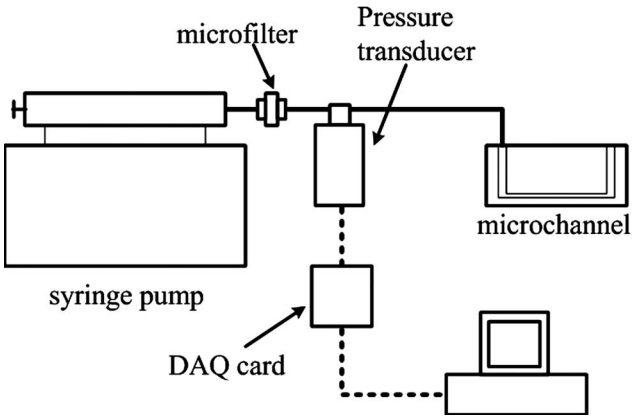

Fig. 2 Schematic of the test section

4 Analysis of Experimental Data

Reynolds number was calculated knowing the volumetric flow rate, Q, and the cross-sectional area, A, from

$$\mathrm{Re}_{\sqrt{A}} = \frac{\rho Q}{\mu \sqrt{A}} \tag{5}$$

Viscous dissipation effect was neglected since the dimensionless number $4\ \mathrm{Ec}[L^* f\ \mathrm{Re}_{\sqrt{A}}]/\mathrm{Re}_{\sqrt{A}} = 0.006$ is much smaller than 1. The value of $\Delta T_{\mathrm{ref}} = 1\,^\circ\mathrm{C}$ was used to calculate the Eckert number, Ec, for water as a working fluid [26]. Hence, the properties of the water was assumed to be constant.

Total measured pressure drop during the experiment, $\Delta P_{\mathrm{measured}}$ is

$$\Delta P_{\mathrm{measured}} = \Delta P_c + \Delta P_{\mathrm{in}} + \Delta P_D + \Delta P_{\mathrm{FD}} + \Delta P_{\mathrm{ex}} + 2\Delta P_b + \Delta P_{\mathrm{ev}} \tag{6}$$

where ΔP_c is the pressure loss due to the flow in the connecting tubes, ΔP_{in} and ΔP_{ex} are the inlet and exit losses, ΔP_D is the developing region loss, ΔP_{FD} is the pressure drop in the fully developed region, ΔP_b is the pressure drop due to 90 deg bends, and ΔP_{ev} is the pressure drop corresponds to the electroviscous effect. Since fully developed pressure drop is the focus of this study, right hand side losses except ΔP_{FD} must be subtracted from the measured pressure drop.

4.1 Connecting Tube Pressure Loss, ΔP_c. The connecting tube pressure drop includes the losses due to all fittings and the capillary tube from the transducer to the microchannel inlet. We measured this loss directly at each flow rate when there was no microchannel at the end of the tubing. The measurements were carefully conducted with the conditions identical to the case when a microchannel was added to the end of the connecting tube to avoid the effects of hydrostatic pressure.

4.2 Developing Region, ΔP_D. Since the viscous boundary layer inherently grows faster in microchannels than in macroscales, the developing region in most cases is negligible. There are few references that can be found in literature, in which the effect of inlet region was considered [40,44,45]. Phillips [44] showed that the length of the hydrodynamic developing region, L_D, depends on the aspect ratio of rectangular cross-section microchannels; the higher the aspect ratio, the longer the developing length. Maximum value of L_D can be obtained from Eq. (7)

$$L_D = \frac{4\varepsilon}{(1+\varepsilon)^2}\frac{\rho Q}{\mu} \tag{7}$$

This equation shows that the developing length depends on the flow rate and the channel aspect ratio. The higher the aspect ratio and/or flow rate, the higher the developing length. Ratio of the maximum developing length over the total length of the microchannel is listed in Table 1 for different channels. Obviously this length occurs in the maximum flow rate. Pressure drop associated with the entrance region after changing the length scale to $\sqrt{A}$ is [46]

$$\Delta P_D = \frac{(f\ \mathrm{Re}_{\sqrt{A}})\mu Q \Gamma}{2A\sqrt{A}} L_D + K\frac{\rho Q^2}{2A^2} \tag{8}$$

where $K = 0.6796 + 1.2197\varepsilon + 3.3089\varepsilon^2 - 9.5921\varepsilon^3 + 8.9089\varepsilon^4$

[3] www.ni.com.

Table 2 Ratio of the developing region pressure drop over the measured pressure drop of the microchannel

	$\Delta P_D/\Delta P_{\text{measured}}$ (%)				
Q (μl/min)	ε=0.13	ε=0.17	ε=0.4	ε=0.6	ε=0.76
40	0.01	0.01	0.04	0.03	0.04
60	0.01	0.02	0.03	0.04	0.06
80	0.01	0.02	0.04	0.06	0.08
100	0.02	0.01	0.06	0.07	0.10
120	0.02	0.02	0.06	0.08	0.11
240	0.03	0.05	0.10	0.20	0.24

$-2.9959\varepsilon^5$.

In Eq. (8), $f\ \mathrm{Re}_{\sqrt{A}}$ was calculated based on the measured pressure drop. Table 2 lists the relative pressure loss of the developing region with respect to the measured pressure drop. As can be seen, the values are small, less than 0.3%, and can be neglected for the range of Reynolds numbers studied in this work ($1<\mathrm{Re}_{\sqrt{A}}<35$). For the higher Reynolds numbers ($\mathrm{Re}\sim 100$), the developing pressure drop, ΔP_D, was found to be less than 2% of the fully developed pressure drop obtained from Eq. (3).

4.3 Minor Losses, ΔP_{min}. Other pressure losses associated with the measured pressure drop are inlet, exit, and bend losses. These losses are usually obtained from the traditional relationships used in macroscale [15,44,46,47]. Phillips [44] showed that the minor pressure losses can be obtained from

$$\Delta P_{\text{min}} = \Delta P_{\text{in}} + \Delta P_{\text{ex}} + 2\Delta P_b = \frac{\rho Q^2}{2A}\left[K_c + K_e + 2K_b\left(\frac{A}{A_t}\right)^2\right] \tag{9}$$

where A and A_t are the channel and connecting tube cross-sectional areas, respectively. K_b is the loss coefficient for the bend, and K_c and K_e represent the contraction and expansion loss coefficients due to area changes. Phillips [44] recommended K_b to be approximately 1.2 for a 90 deg bend. Assuming equal cross-sectional areas for the channel and connecting tubes and also maximum possible values for K_c and K_e [48], relative minor losses with respect to the measured pressure drop are listed in Table 3. As can be seen, these losses are negligible compared with the measured pressure drop. For higher Reynolds numbers ($\mathrm{Re}\sim 100$), minor pressure drop, ΔP_{min}, was found to be less than 5% of the fully developed pressure drop obtained from Eq. (3).

4.4 Electroviscous Effect, ΔP_{ev}. When a liquid is forced through a narrow channel under an applied pressure gradient, the counterions in the diffusive layer of EDL (electric double layer) are moving toward the downstream end and a potential gradient is induced in the flow [49]. This so called streaming potential acts to drive the counterions in the diffuse layer of the EDL to move in the direction opposite to the pressure-driven flow. The overall result is a reduced flow rate for a constant pressure gradient or increase in pressure drop for a given flow rate. This phenomenon, which gives the appearance of an increased viscosity, μ_a, is called the electroviscous effect [50]. The ratio of this apparent viscosity to the actual fluid viscosity for circular cross-section capillaries can be found from [50]

$$\frac{\mu_a}{\mu} \approx 1 + \frac{32\mu}{\sigma_b D^2}\mu_{\text{eo}}^2 \tag{10}$$

where D is the capillary diameter, μ is the fluid viscosity, σ_b is the liquid electrical conductivity, and a is the radius of the capillary. $\mu_{\text{eo}}=\varepsilon_0\varepsilon_r\zeta/\mu$ is the electro-osmotic mobility, where $\varepsilon_0=8.854\times10^{-12}$ $\mathrm{C^2\ V^{-1}\ m^{-1}}$ is the permittivity of vacuum, $\varepsilon_r=78.3$ is the relative permittivity for water at 25°C [49], and ζ is the zeta potential of the surface. Approximating the rectangular cross-section microchannel with a capillary of the same cross-sectional area, $\sigma_b=5.6\times10^{-6}$ $\mathrm{S\ m^{-1}}$ [51] and $\mu_{\text{eo}}=5.9\times10^{-8}$ $\mathrm{m^2\ V^{-1}\ s^{-1}}$ [52] for PDMS, value of μ_a/μ was found to be less than 1.03 for the channel sizes in this study.

Table 3 Ratio of the minor pressure loss over the measured pressure drop of the microchannel

	$\Delta P_{\text{min}}/\Delta P_{\text{measured}}$ (%)				
Q (μl/min)	ε=0.13	ε=0.17	ε=0.4	ε=0.6	ε=0.76
40	0.04	0.04	0.12	0.09	0.11
60	0.05	0.07	0.10	0.13	0.17
80	0.07	0.10	0.14	0.17	0.23
100	0.08	0.07	0.21	0.22	0.28
120	0.09	0.10	0.19	0.25	0.35
240	0.16	0.24	0.35	0.51	0.70

4.5 Effect of Channel Deformation Under Pressure-Driven Flow. Effect of channel deformation becomes important since it can change the microchannel cross-sectional area and as a result the pressure drop. In all equations used in Secs. 1–3, we assumed that the channel cross section did not change under pressure-driven flow. Few works have discussed the importance of bulk deformation in rectangular microchannels. Holden et al. [53] measured the PDMS bulk deformation under high pressure drops ($\sim$1 bar) using the change in fluorescence intensity. Gervais et al. [54] studied the elastic deformation of PDMS microchannels under imposed flow rates. They demonstrated that the channel deformation can effect the the laminar flow profile and pressure distribution within the channels with low aspect ratios and high pressure drops. In a bulged microchannel, measured pressure drop no longer changes linearly with the flow rate [53]. This is because the microchannel cross section varies due to deformation, and for a constant flow rate, pressure drop changes. Figure 3 shows the variation in the channel pressure drop with flow rate for present work. Experimental results properly follow the linear behavior of theoretical profiles. Thus one can conclude that the channel deformation has negligible effect on the results in this work. However, a careful experimental and theoretical investigation is required to study the effect of the channel deformation on the pressure drop of moderate and high aspect ratio rectangular cross-section microchannels.

4.6 Uncertainty Analysis. A careful analysis of the experimental uncertainty in this study is critical to the interpretation of experimental data of Poiseuille number, Po, and exploration of deviations from the macroscale theory. Neglecting the developing region, minor losses, electroviscous effects, and considering that the channel deformation is not significant, the experimental Poiseuille number can be obtained from

$$\mathrm{Po}_{\text{exp}} = \frac{4}{\mu Q}\left(\frac{A^2\sqrt{A}}{L\Gamma}\right)\Delta P_{\text{FD}} \tag{11}$$

where $\Delta P_{\text{FD}}=\Delta P_{\text{measured}}-\Delta P_c$. The uncertainty associated with Po_{exp} based on the measured variables, and the method provided in Ref. [43] is then given by

$$\frac{\omega_{\mathrm{Po}_{\text{exp}}}}{\mathrm{Po}_{\text{exp}}} = \left[\left(\frac{\omega_{\Delta P}}{\Delta P}\right)^2 + \left(\frac{\omega_L}{L}\right)^2 + \left(\frac{\omega_\Gamma}{\Gamma}\right)^2 + \frac{25}{4}\left(\frac{\omega_A}{A}\right)^2 + \left(\frac{\omega_Q}{Q}\right)^2\right]^{1/2} \tag{12}$$

where ω values indicate uncertainty associated with each variable as subscribed, $\omega_A=4[(H\omega_W)^2+(W\omega_H)^2]^{1/2}$ and $\omega_\Gamma=4[\omega_W^2+\omega_H^2]^{1/2}$ (see Appendix for details of calculations). In this equation we

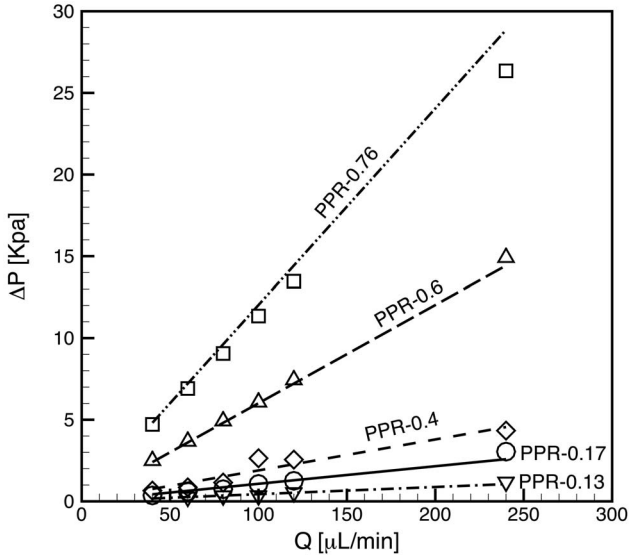

Fig. 3 Channel pressure drop as a function of flow rate. Lines show the theoretical prediction of pressure drop using Eq. (3) and symbols show the experimental data.

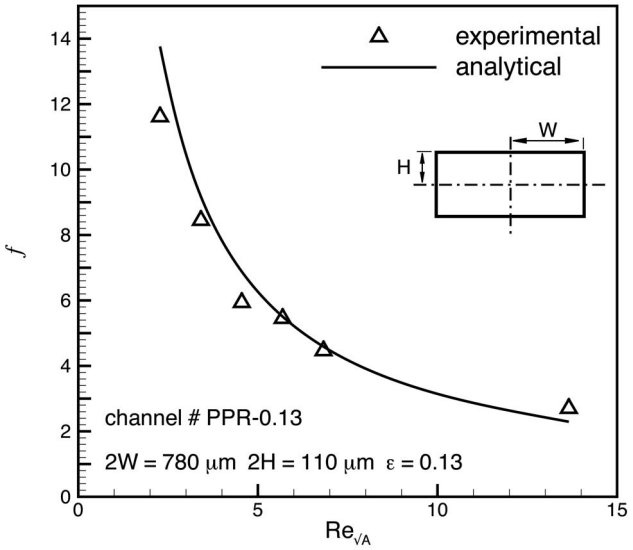

Fig. 4 Variation in friction factor with Reynolds number for sample no. PPR-0.13

assumed that the fluid properties remained constant. Equation (12) shows that the channel dimensions play an important role in determination of uncertainty by effecting three terms. Also for small Reynolds numbers, the accuracy of the flow rate becomes more significant. The uncertainty in the measurement of each parameter is listed in Table 4. Using Eq. (12) minimum uncertainties for the samples of PPR-0.13, PPR-0.17, PPR-0.4, PPR-0.6, and PPR-0.76 are 8.7%, 9.3%, 8.9%, 9.3%, and 11.1%, respectively.

5 Results and Discussion

Figures 4 and 5 show the comparison between friction factor obtained from Eq. (3), the solid line, and experimental data for two typical samples of PPR-0.13 and PPR-0.76, respectively. As shown, the trend and the values of experimental data are well predicted by the theoretical model. Consistent with the laminar flow in channels friction factor decreases with the Reynolds number.

Variation in the Poiseuille number, $f\ \mathrm{Re}_{\sqrt{A}}$, with the Reynolds number for different channels is shown in Fig. 6. Experimental data are normalized by the analytical model obtained from Eq. (3). The solid line shows the analytical model. From Eq. (3), it is clear that the Poiseuille number does not depend on the Reynolds number and it only varies with the aspect ratio of the channel cross section. The same trend can be observed in the experimental data. Large deviations from this trend in the very low Reynolds numbers attributed to the large uncertainties occur due to small flow rates and pressure drops. The Reynolds number can be a result of the small cross-sectional area and/or flow rate, with both parameters increasing the uncertainty in the value of the Poiseuille number, see Eq. (12). As can be seen, most of the experimental points fall within ±10% bounds of the analytical model.

Table 4 Uncertainty values for measured parameters

Parameter	Uncertainty
ΔP	±0.25% of full scale
L	±0.02 mm
W	±3.6 μm
H	±3.6 μm
Q	±0.5%

Another comparison of the present experimental work with analytical model is illustrated in Fig. 7. Since the Poiseuille number, $f\ \mathrm{Re}_{\sqrt{A}}$, remains constant for the laminar regime as the Reynolds number varies, the experimental data for each set were averaged over the laminar region. The ±10% bounds of the model are also shown in the plot to better demonstrate the agreement between the data and the model.

As shown in Eq. (3), the Poiseuille number, $f\ \mathrm{Re}_{\sqrt{A}}$, is only a function of the aspect ratio, which is a geometrical parameter. This dependency is plotted in Fig. 8. Averaged values over the studied range of the Reynolds number were used in this plot. It can be observed that for smaller aspect ratios, the Poiseuille number, $f\ \mathrm{Re}_{\sqrt{A}}$, increases sharply. To better show the trend of the analytical model, two asymptotes of very narrow and square cross sections are also included in Fig. 8. As can be seen, when $\varepsilon \to 0$, parallel plate, the Poiseuille number asymptotically approaches $4\pi^2/3\sqrt{\varepsilon}$.

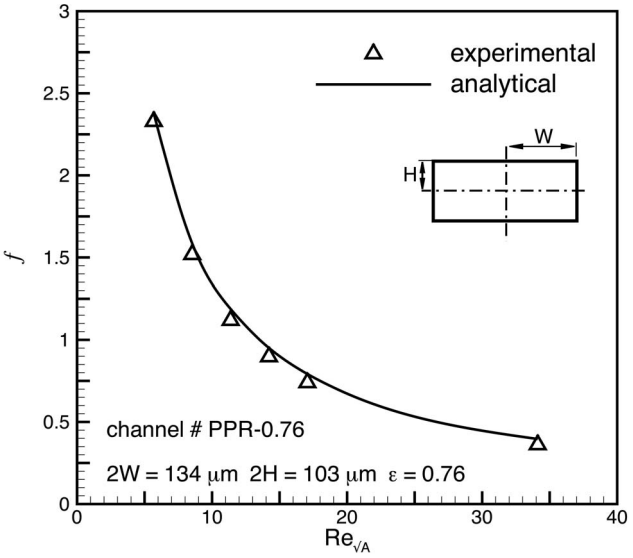

Fig. 5 Variation in friction factor with Reynolds number for sample no. PPR-0.76

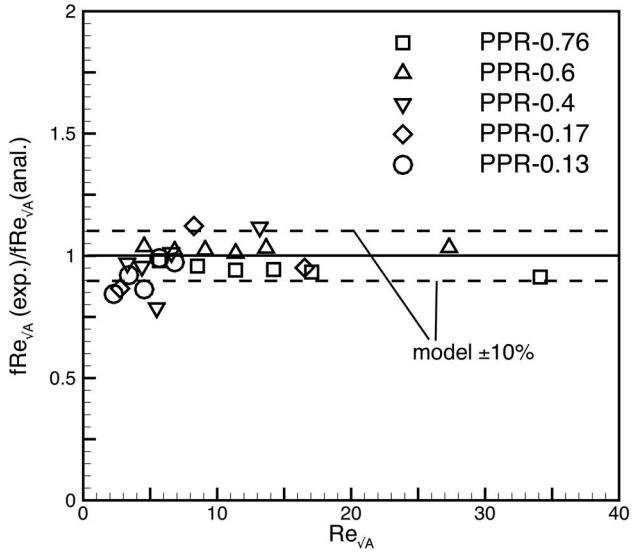

Fig. 6 Variation in Poiseuille number, $f\ \mathrm{Re}_{\sqrt{A}}$, with Reynolds number

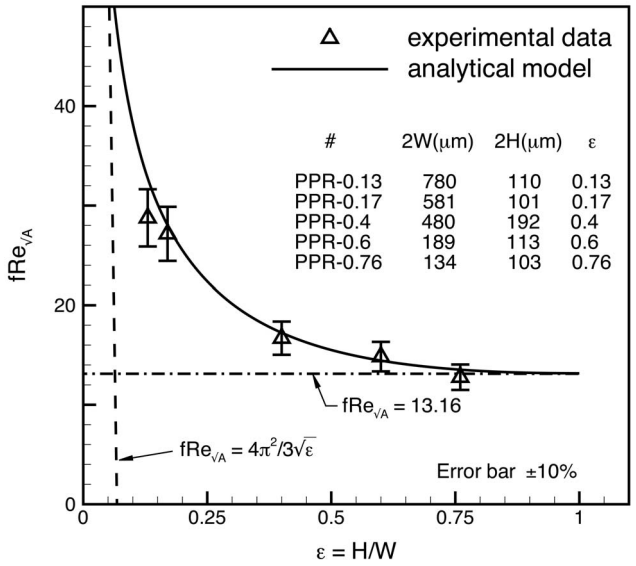

Fig. 8 Variation in Poiseuille number, $f\ \mathrm{Re}_{\sqrt{A}}$, with Reynolds number

It is beneficial to compare the results of present work with the existing data of rectangular microchannels. Data were collected from the works of Wu and Cheng [31], Lu and Garimella [32], and Gao et al. [33]. As shown in Fig. 9, the collected data cover a wide range of the aspect ratio for almost three decades. The solid line represents the analytical model of Bahrami et al. [1]. As can be seen, the analytical model agrees well with the experimental data over the wide range of microchannel cross-section aspect ratio.

6 Summary and Conclusions

The general model developed by Bahrami et al. [1,36] was experimentally validated for the case of rectangular cross-section microchannels. Frictional pressure drop measurements were conducted over a range of Reynolds numbers from 1 to 35 for rectangular cross-section microchannels fabricated with soft lithography method in the aspect ratio range of $0.13 < \varepsilon < 0.76$. A careful measurement of pressure drop and channel dimensions was conducted, and the pressure drops due to the developing region, minor losses, and electroviscous effect were estimated using available models in literature. Channel deformation due to the pressure inside the microchannel was found to be negligible since the pressure drop changes linearly with the flow rate. Comparing the results with the general theoretical model shows good agreement between the model and experimental data.

Uncertainty analysis showed that the measurement of channel dimensions and flow rate is critical in microscales. Here, microchannel cross-section geometry was determined through processing high quality images of the channel cross section.

According to the analytical model and experimental data of present work, the Poiseuille number, $f\ \mathrm{Re}_{\sqrt{A}}$, was found to be only a function of microchannel geometry in the range of Reynolds numbers studied in this work. For rectangular cross sections, the channel aspect ratio is the only parameter that affects the Poi-

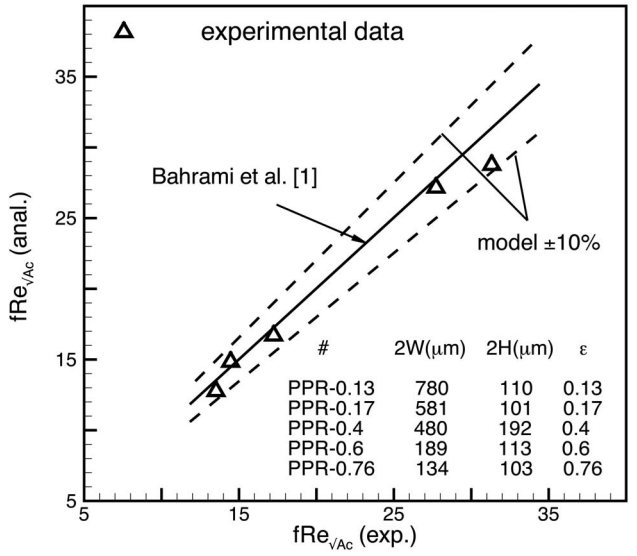

Fig. 7 Comparison of experimental data of present work with analytical model of Bahrami et al. [1]

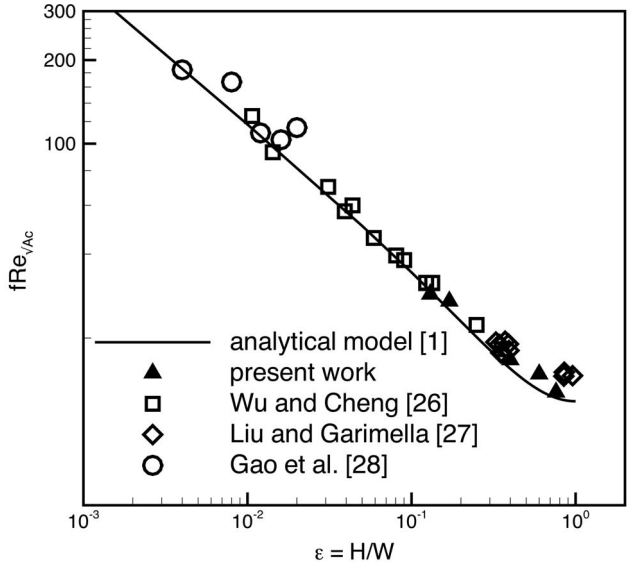

Fig. 9 Comparison between experimental data of present study and previous works

seuille number. The analytical model employed in this work will be applied to other channel geometries such as variable cross-section microchannels in our future work.

Acknowledgment

The authors gratefully acknowledge the financial support of the Natural Sciences and Engineering Research Council of Canada (NSERC). Also they thank Dr. Viatcheslav Berejnov and Mr. Ali K. Oskooi for their assistance.

Nomenclature

A = microchannel cross-sectional area, m^2
A_t = tubing cross-sectional area, m^2
c_p = fluid specific heat, J/kg K
Ec = Eckert number, $W^2/(2c_p\Delta T_{\text{ref}})$
f = Fanning friction factor
H = channel half height, m
I_p = polar momentum of inertia, m^4
I_p^* = specific polar momentum of inertia, I_p/A^2
K_b = loss coefficient for bend
K_c = flow contraction loss coefficient
K_e = flow expansion loss coefficient
L = channel length, m
L_D = developing region length, m
L^* = dimensionless length $L/\sqrt{A}$
Po = Poiseuille number, $f\ \text{Re}_{\sqrt{A}}$
Q = volumetric flow rate, m^3/s
$\text{Re}_{\sqrt{A}}$ = Reynolds number, $\rho Q/\mu\sqrt{A}$
W = channel half width, m

Greek

ΔP_b = bend pressure loss, Pa
ΔP_c = connecting tube pressure loss, Pa
ΔP_D = developing region pressure loss, Pa
ΔP_{ex} = exit pressure loss, Pa
ΔP_{FD} = fully developed pressure loss, Pa
ΔP_{ev} = pressure loss due to electroviscous effect, Pa
ΔP_{in} = inlet pressure loss, Pa
ε = channel aspect ratio, $2H/2W$
Γ = channel cross-section perimeter, m
μ = fluid viscosity, kg/m s
μ_a = apparent viscosity, kg/m s
μ_{eo} = electro-osmotic mobility, m^2/V s
ρ = fluid density, kg/m^3
σ_b = fluid electrical conductivity, S/m
ω = uncertainty

Appendix: Uncertainty Formulation

To calculate the uncertainty associated with the experimental measurements the following relation is used [43]:

$$\omega_R = \left[\sum \left(\frac{\partial R}{\partial x_i}\omega_i\right)^2\right]^{1/2} \tag{A1}$$

where ω_R is the uncertainty in results, $R(x_1, x_2, \ldots, x_n)$, and ω_i is the uncertainty of the independent variable x_i. If the results function, $R(x_1, x_2, \ldots, x_n)$, takes the form of a product of the independent variables, $R = x_1^{a_1} x_2^{a_2}, \ldots, x_n^{a_n}$, Eq. (A1) can be rewritten as

$$\frac{\omega_R}{R} = \left[\sum \left(\frac{a_i}{x_i}\omega_i\right)^2\right]^{1/2} \tag{A2}$$

The final form of the uncertainty of the Poiseuille number, Eq. (12), is obtained using Eqs. (10) and (A2).

To calculate the uncertainty of the channel cross section, $A = 4W \times H$, and perimeter, $\Gamma = 4(W+H)$, Eq. (A1) is employed

$$\omega_A = \left[\left(\frac{\partial A}{\partial W}\omega_W\right)^2 + \left(\frac{\partial A}{\partial H}\omega_H\right)^2\right]^{1/2} \tag{A3}$$

$$\omega_\Gamma = \left[\left(\frac{\partial \Gamma}{\partial W}\omega_W\right)^2 + \left(\frac{\partial \Gamma}{\partial H}\omega_H\right)^2\right]^{1/2} \tag{A4}$$

where $\partial A/\partial W = 4H$, $\partial A/\partial H = 4W$, $\partial \Gamma/\partial W = 4$, and $\partial \Gamma/\partial H = 4$.

References

[1] Bahrami, M., Yovanovich, M. M., and Culham, J. R., 2006, "Pressure Drop of Laminar, Fully Developed Flow in Microchannels of Arbitrary Cross-Section," ASME J. Fluids Eng., **128**, pp. 1036–1044.
[2] Whitesides, G. M., 2006, "The Origins and the Future of Microfluidics," Nature (London), **442**, pp. 368–372.
[3] Grushka, E., McCormick, R. M., and Kirkland, J. J., 1989, "Effect of Temperature Gradients on the Efficiency of Capillary Zone Electrophoresis Separations," Anal. Chem., **61**, pp. 241–246.
[4] Fletcher, P. D. I., Haswell, S. J., Pombo-Villar, E., Warrington, B. H., Watts, P., Wong, S., and Zhang, X., 2002, "Micro Reactors: Principles and Applications in Synthesis," Tetrahedron, **58**, pp. 4735–4757.
[5] DeWitt, S., 1999, "Microreactors for Chemical Synthesis," Curr. Opin. Chem. Biol., **3**(3), pp. 350–356.
[6] Miyake, R., Lammerink, S. J., Elwenspoek, M., and Fluitman, H. J., 1993, "Micro Mixer With Fast Diffusion," MEMS '93, Fort Lauderdale, FL, pp. 248–253.
[7] Weigl, B. H., Bardell, R. L., and Cabrera, C. R., 2003, "Lab-on-a-Chip for Drug Development," Adv. Drug Delivery Rev., **55**, pp. 349–377.
[8] Becker, H., and Locascio, L. E., 2002, "Polymer Microfluidic Devices," Talanta, **56**, pp. 267–287.
[9] Chovan, T., and Guttman, A., 2002, "Microfabricated Devices in Biotechnology and Biochemical Processing," Trends Biotechnol., **20**(3), pp. 116–122.
[10] Ehrfeld, W., 2003, "Electrochemistry and Microsystems," Electrochim. Acta, **48**, pp. 2857–2868.
[11] Bayraktar, T., and Pidugu, S. B., 2006, "Characterization of Liquid Flows in Microfluidic Systems," Int. J. Heat Mass Transfer, **49**, pp. 815–824.
[12] Peng, X. F., Peterson, G. P., and Wang, B. X., 1994, "Frictional Flow Characteristics of Water Flowing Through Rectangular Microchannels," Exp. Heat Transfer, **7**, pp. 249–64.
[13] Xu, B., Ooi, K. T., and Wong, N. T., 2000, "Experimental Investigation of Flow Friction for Liquid Flow in Microchannels," Int. Commun. Heat Mass Transfer, **27**, pp. 1165–1176.
[14] Ren, C. L., and Li, D., 2004, "Electroviscous Effects on Pressure-Driven Flow of Dilute Electrolyte Solutions in Small Microchannels," J. Colloid Interface Sci., **274**, pp. 319–330.
[15] Judy, J., Maynes, D., and Webb, B. W., 2002, "Characterization of Frictional Pressure Drop for Liquid Flows Through Microchannels," Int. J. Heat Mass Transfer, **45**, pp. 3477–3489.
[16] Tuckerman, D. B., and Peace, R. F. W., 1981, "High-Performance Heat Sinking for VLSI," IEEE Electron Device Lett., **2**, pp. 126–129.
[17] Mala, G. M., and Li, D., 1999, "Flow Characteristics of Water in Microtubes," Int. J. Heat Mass Transfer, **20**, pp. 142–148.
[18] Pfhaler, J., Harley, J., and Bau, H., 1990, "Liquid Transport in Micron and Submicron Channels," Sens. Actuators, A, **A21–A23**, pp. 431–434.
[19] Pfhaler, J., Harley, J., Bau, H., and Zemel, J. N., 1991, "Gas and Liquid Flow in Small Channels Micromechanical Sensors, Actuators, and Systems," ASME Dyn. Syst. Control Div., **32**, pp. 49–60.
[20] Urbanek, W., Zemel, J. N., and Bau, H. H., 1993, "An Investigation of the Temperature Dependence of Poiseuille Numbers in Microchannel Flow," J. Micromech. Microeng., **3**, pp. 206–208.
[21] Qu, W., Mala, G. M., and Li, D., 2000, "Pressure-Driven Water Flows in trapezoidal Silicon Microchannels," Int. J. Heat Mass Transfer, **43**, pp. 3925–3936.
[22] Papautsky, I., Brazzle, J., Ameel, T., and Frazier, A. B., 1999, "Laminar Fluid Behavior in Microchannels Using Micropolar Fluid Theory," Sens. Actuators, A, **73**, pp. 101–108.
[23] Ren, C. L., and Li, D., 2005, "Improved Understanding of the Effect of Electrical Double Layer on Pressure-Driven Flow in Microchannels," Anal. Chim. Acta, **531**, pp. 15–23.
[24] Weilin, Q., Mala, H. M., and Li, D., 2000, "Pressure-Driven Water Flows in Trapezoidal Silicon Microchannels," Int. J. Heat Mass Transfer, **43**, pp. 353–364.
[25] Guo, Z., and Li, Z., 2003, "Size Effect on Microscale Single-Phase Flow and Heat Transfer," Int. J. Heat Mass Transfer, **46**, pp. 149–159.
[26] Morini, G. L., 2005, "Viscous Heating in Liquid Flows in Microchannels," Int. J. Heat Mass Transfer, **48**, pp. 3637–3647.
[27] Bahrami, M., Yovanovich, M. M., and Culham, J. R., 2006, "Pressure Drop of Laminar, Fully Developed Flow in Rough Microtubes," ASME J. Fluids Eng., **128**, pp. 632–637.
[28] Jiang, X. N., Zhou, Z. Y., Huang, X. Y., and Liu, C. Y., 1997, "Laminar Flow Through Microchannels Used for Microscale Cooling Systems," IEEE/CPMT Electronic Packaging Technology Conference, pp. 119–122.
[29] Baviere, R., Ayela, F., Le Person, S., and Favre-Marinet, M., 2005, "Experimental Characterization of Water Flow Through Smooth Rectangular Microchannels," Phys. Fluids, **17**, p. 098105.
[30] Bucci, A., Celata, G. P., Cumo, M., Serra, E., and Zummo, G., 2003, "Water Single-Phase Fluid Flow and Heat Transfer in Capillary Tubes," International Conference on Microchannels and Minichannels, Vol. 1, pp. 319–326, ASME Paper No. 1037.

[31] Wu, H. Y., and Cheng, P., 2003, "Friction Factors in Smooth Trapezoidal Silicon Microchannels With Different Aspect Ratios," Int. J. Heat Mass Transfer, **46**, pp. 2519–2525.
[32] Liu, D., and Garimella, S., 2004, "Investigation of Liquid Flow in Microchannels," J. Thermophys. Heat Transfer, **18**, pp. 65–72.
[33] Gao, P., Le Person, S., and Favre-Marinet, M., 2002, "Scale Effects on Hydrodynamics and Heat Transfer in Two-Dimensional Mini and Microchannels," Int. J. Therm. Sci., **41**, pp. 1017–1027.
[34] Squires, T. M., and Quake, S. R., 2005, "Micro Fluidics: Fluid Physics at Nanoliter Scale," Rev. Mod. Phys., **77**, pp. 977–1026.
[35] White, F. M., 1974, *Viscous Fluid Flow*, McGraw-Hill, New York, Chap. 3.
[36] Bahrami, M., Yovanovich, M. M., and Culham, J. R., 2007, "A Novel Solution for Pressure Drop in Singly Connected Microchannels," Int. J. Heat Mass Transfer, **50**, pp. 2492–2502.
[37] Timoshenko, S. P., and Goodier, J. N., 1970, *Theory of Elasticity*, McGraw-Hill, New York, Chap. 10.
[38] Yovanovich, M. M., 1974, "A General Expression for Predicting Conduction Shape Factors," *AIAA Prog. in Astro. and Aeronautics: Thermophysics and Space Craft Control*, Vol. 35, R. G. Hering, ed., MIT Press, Cambridge, MA, pp. 265–291.
[39] Muzychka, Y. S., and Yovanovich, M. M., 2002, "Laminar Flow Friction and Heat Transfer in Non-Circular Ducts and Channels Part 1: Hydrodynamic Problem," Proceedings of Compact Heat Exchangers, A Festschrift on the 60th Birthday of Ramesh K. Shah, Grenoble, France, pp. 123–130.
[40] Shah, R. K., and London, A. L., 1978, *Laminar Flow Forced Convection in Ducts, Supplement to Advances in Heat Transfer*, Academic, New York.
[41] Erickson, D., Sinton, D., and Li, D., 2003, "Joule Heating and Heat Transfer in Poly(dimethylsiloxane) Microfluidic Systems," Lab Chip, **3**, pp. 141–149.
[42] McDonald, J. C., Duffy, D. C., Anderson, J. R., Chiu, D. T., Wu, H., Schueller, O. J. A., and Whiteside, G., 2000, "Fabrication of Microfluidic Systems in Poly(dimethylsiloxane)," Electrophoresis, **21**, pp. 27–40.
[43] Holman, J. P., 2001, *Experimental Methods for Engineering*, 7th ed., McGraw-Hill, New York, Chap. 3.
[44] Phillips, R. J., 1990, *Microchannel Heat Sinks, Advances in Thermal Modeling of Electronic Components and Systems*, Hemisphere, New York, Chap. 3.
[45] Sharp, K. V., Adrian, R. J., Santiago, J. G., and Molho, J. I., 2005, *Liquid Flows in Microchannels, MEMS Hand Book: Introduction and Fundamentals*, 2nd ed., Taylor & Francis, New York.
[46] Kandlikar, S. G., Garimella, S., Li, D., Colin, S., and King, M. R., 2006, *Heat Transfer and Fluid Flow in Minichannels and Microchannels*, Elsevier, Oxford.
[47] Steinke, M. E., and Kandlikar, S. G., 2006, "Single-Phase Liquid Friction Factors in Microchannels," Int. J. Therm. Sci., **45**, pp. 1073–1083.
[48] Kays, W. M., and London, A. L., 1984, *Compact Heat Exchangers*, McGraw-Hill, New York.
[49] Probstein, R. F., 1994, *Physicochemical Hydrodynamics*, 2nd ed., Wiley, New York.
[50] Masliyah, J. H., and Bhattacharjee, S., 2006, *Electrokinetic and Colloid Transport Phenomena*, Wiley, Englewood Cliffs, NJ.
[51] Lide, D., and Kehiaian, H. V., 1994, *CRC Handbook of Thermophysical and Thermochemical Data*, 1st ed., CRC Press, Florida.
[52] Lee, J. S. H., Hu, Y., and Li, D., 2005, "Electrokinetic Concentration Gradient Generation Using a Converging-Diverging Microchannel," Anal. Chim. Acta, **543**, pp. 99–108.
[53] Holden, M. A., Kumar, S., Beskok, A., and Cremer, P. S., 2003, "Microfluidic Diffusion Diluter: Bulging of PDMS Microchannels Under Pressure Driven Flow," J. Micromech. Microeng., **13**, pp. 412–418.
[54] Gervais, T., El-Ali, J., Gunther, A., and Jensen, K., 2006, "Flow-Induced Deformation of Shallow Microfluidic Channels," Lab Chip, **6**, pp. 500–507.